FRONTIERS OF PHYSICS

RESEARCH ARTICLE
Volume 17 / Issue 5 / 52506 / 2022

Generalized high-order twisted partially coherent beams and their propagation characteristics

Hai-Yun Wang[1], Zhao-Hui Yang[1], Kun Liu[1], Ya-Hong Chen[1], Lin Liu[1,†], Fei Wang[1,‡], Yang-Jian Cai[1,2,§]

1 School of Physical Science and Technology & Collaborative Innovation Center of Suzhou Nano Science and Technology, Soochow University, Suzhou 215006, China
2 Shandong Provincial Engineering and Technical Center of Light Manipulations & Shandong Provincial Key Laboratory of Optics and Photonic Devices, School of Physics and Electronics, Shandong Normal University, Jinan 250014, China
Corresponding authors. E-mail: †liulin@suda.edu.cn, ‡fwang@suda.edu.cn, §yangjian_cai@163.com
Received April 12, 2022; accepted July 26, 2022

ABSTRACT

Twist phase is a nontrivial statistical phase that only exists in partially coherent fields, which makes the beam carry orbital angular momentum (OAM). In this paper, we introduce a new kind of partially coherent beams carrying high-order twist phase, named generalized high-order twisted partially coherent beams (GHTPCBs). The propagation dynamics such as the spectral density and OAM flux density propagating in free space are investigated numerically with the help of mode superposition and fast Fourier transform (FFT) algorithm. Our results show that the GHTPCBs are capable of self-focusing, and the beam spot during propagation exhibits teardrop-like or the diamond-like shape in some certain cases. Moreover, the influences of the twist order and the twist factor on the OAM flux density during propagation are also illustrated in detail. Finally, we experimentally synthesize the GHTPCBs with controllable twist phase by means of pseudo-mode superposition and measure their spectral density during propagation. The experimental results agree well with the theoretical predictions. Our studies may find applications in nonlinear optics and particle trapping.

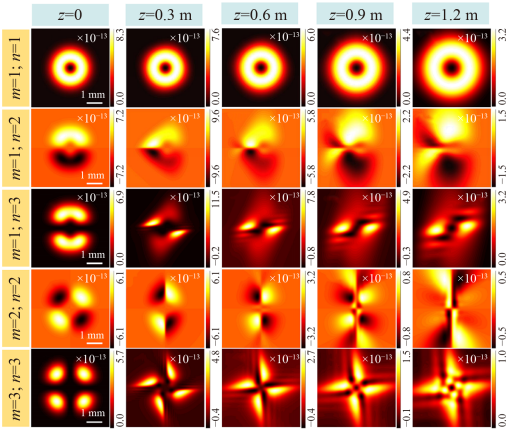

Keywords light manipulation, statistical optics, twist phase, coherence structure, orbital angular momentum

1 Introduction

Twist phase is a second-order statistical quadratic phase that depends on two spatial points and cannot be separated with respect to two positions, expressed as $\exp[iu(x_1y_2 - x_2y_1)]$, where u is the twist factor, a measure of the strength of the phase; (x_i, y_i), $i = 1, 2$, are two position vectors. Different from the vortex phase and spherical phase, the twist phase only survives in partially coherent light. In 1993, Simon *et al.* first introduced such twist phase into a Gaussian Schell-model beam which is the well-known class of partially coherent beams [1]. It was found that the twist phase has intrinsic chiral or handedness property, responsible for the rotation of beam spot during propagation [1, 2]. As a new degree of freedom to manipulate the partially coherent light, the twist phase has attracted considerable attention in recent years. Various methods such as the coherent mode decomposition, Wigner distribution function and efficient tensor method have been proposed to treat the propagation of

https://doi.org/10.1007/s11467-022-1196-8

the beams carrying the twist phase [3–6].

Recently, Borghi *et al.* [7, 8] proposed a criterion to judge whether the twist phase can impose on partially coherent beams with different degree of coherences (DOCs). Gori *et al.* [9, 10] established a condition to construct twisted partially coherent beam with physically realizable. Since then, twisted beams with different kinds of DOCs have been introduced, and their propagation characteristics in free space and turbulent atmosphere were investigated [11–17]. The twisted beams have found important applications in many aspects such as ghost imaging [18], controlling the coherence of optical solitons [19], reducing the turbulence-induced scintillation index [20], overcoming the Rayleigh limit in imaging system [21], generating highly incoherent yet highly entangled multiphoton states [22], realizing phase conjugation in stimulated down-conversion [23], and others. Meanwhile, many experimental setups have been established to generate and measure the twisted partially coherent beams [2, 24–26], these methods have provided a strongly experimental basis for the application of twisted partially coherent beams.

Perhaps the most peculiar property of the twist phase is that such phase induces the beam carrying orbital angular momentum (OAM) [26–28]. In 2001, Serna *et al.* [27] pointed out that twisted Gaussian Schell-model (TGSM) beams carrying the non-zero time average OAM along propagation direction, opens up a new dimension for manipulating OAM in partially coherent fields. Later, the changes of total OAM of the TGSM beams propagation through a gain/loss cavity and a uniaxial crystal were investigated in detail [29, 30]. The OAM flux density of the TGSM beams exhibit the fluid rotators with a rigid body in the beam center and a constant flux density at the outskirt [28], which is similar with that of beams carrying vortex phase.

However, most of the studies are focused on the low-order twist phase, i.e., quadratic non-separable phase stated above. Recently, Wan and Zhao [31] introduced a high-order twist phase in partially coherent fields, which is $\exp\left[\mathrm{i}u\left(x_1^m y_2^m - x_2^m y_1^m\right)\right]$, where m is an integer number. Such phase only exists in partially coherent beams with spatially varying coherence state. Up to now, the experimental generation of the beams with high-order twist phase have not been reported. In this paper, we extend the high-order twist phase to a more general case, i.e., the powers on $x_{1(2)}$ and $y_{1(2)}$ are different, and the partially coherent beams carrying such generalized high-order twist phase, named generalized high-order twisted partially coherent beams (GHTPCBs), are constructed theoretically. The propagation dynamics including average spectral density and OAM flux density upon free-space propagating are investigated numerically. Further, an experimental setup for the generation of the GHTPCBs is established. The effects of the high-order twist phase on the propagation dynamics of the generated GHTPCBs are examined in experiment.

2 Theoretical models of GHTPCBs

Consider a scalar, statistically stationary beam-like field, propagating along z-axis. The second-order statistics of such beam in the source plane ($z = 0$) can be characterized by a two-point cross-spectral density (CSD) function in space frequency domain

$$W_0\left(\boldsymbol{r}_1, \boldsymbol{r}_2\right) = \left\langle E^*\left(\boldsymbol{r}_1\right) E\left(\boldsymbol{r}_2\right)\right\rangle, \tag{1}$$

where $\boldsymbol{r}_1 = (x_1, y_1)$ and $\boldsymbol{r}_2 = (x_2, y_2)$ are two position vectors in the source plane, perpendicular to the propagation axis. $E(\boldsymbol{r})$ denotes the random electric filed. The asterisk and the angle brackets stand for the complex conjugate and ensemble average over the source fluctuations, respectively.

To be a genuine CSD function, the necessary and sufficient condition is that the CSD can be expressed as the following alternative integral form [9]

$$W_0\left(\boldsymbol{r}_1, \boldsymbol{r}_2\right) = \int_{-\infty}^{\infty} p(\boldsymbol{v})\, H_0^*\left(\boldsymbol{r}_1, \boldsymbol{v}\right) H_0\left(\boldsymbol{r}_2, \boldsymbol{v}\right) \mathrm{d}^2\boldsymbol{v}, \tag{2}$$

where $p(\boldsymbol{v})$ is a non-negative weight function and $H_0(\boldsymbol{r}, \boldsymbol{v})$ is an arbitrary kernel function. If the kernel function $H_0(\boldsymbol{r}, \boldsymbol{v})$ is the Fourier kernel $\exp(\mathrm{i}a\boldsymbol{r}\cdot\boldsymbol{v})$, where a is a real constant, it represents the Schell-model beams, a well-known class of partially coherent beams. In order to introduce a high-order twist phase, one may employ the kernel function as the form

$$\begin{aligned} H_0\left(\boldsymbol{r}, \boldsymbol{v}\right) =& \tau(\boldsymbol{r}) \exp\left[-\frac{2\alpha^2}{\beta}\left(\frac{x^{2m}}{x_0^{2m-2}} + \frac{y^{2n}}{y_0^{2n-2}}\right)\right] \\ & \times \exp\left[2\alpha\left(\frac{x^m}{x_0^{m-1}} v_x + \frac{y^n}{y_0^{n-1}} v_y\right)\right] \\ & \times \exp\left[-\mathrm{i}\gamma\left(\frac{y^n}{y_0^{n-1}} v_x - \frac{x^m}{x_0^{m-1}} v_y\right)\right], \end{aligned} \tag{3}$$

where $\tau(\boldsymbol{r}) = \exp\left(-\boldsymbol{r}^2/4\sigma_0^2\right)$ is an amplitude function with σ_0 being the beam width. Here, α, β and γ are real constants with inverse square length dimensions. x_0 and y_0 are also real constants with length dimensions. m and n are positive integers that determine the order of the twist phase. Suppose that the $p(\boldsymbol{v})$ function is a Gaussian function, given by

$$p(\boldsymbol{v}) = \frac{\beta}{\pi} \exp\left[-\beta\left(v_x^2 + v_y^2\right)\right]. \tag{4}$$

The $p(\boldsymbol{v})$ function is non-negative for any $\boldsymbol{v}$, which implies that $\beta \geq 0$. Substitution Eqs. (3) and (4) into Eq. (2), and after some integral operations, we obtain the expression for the CSD function

$$W_0(\boldsymbol{r}_1,\boldsymbol{r}_2)=\exp\left(-\frac{\boldsymbol{r}_1^2+\boldsymbol{r}_2^2}{4\sigma_0^2}\right)\times\exp\left[-\frac{(x_1^m-x_2^m)^2}{\delta_{0x}^{2m}}-\frac{(y_1^n-y_2^n)^2}{\delta_{0y}^{2n}}\right]\times\exp\left[-\mathrm{i}u\left(x_1^m y_2^n-x_2^m y_1^n\right)\right],\tag{5}$$

with $1/\delta_{0x}^{2m}=\left(4\alpha^2+\gamma^2\right)/\left(4\beta x_0^{2m-2}\right)$, $1/\delta_{0y}^{2n}=\left(4\alpha^2+\gamma^2\right)/\left(4\beta y_0^{2n-2}\right)$ and $u=2\alpha\gamma/\left(\beta x_0^{m-1}y_0^{n-1}\right)$, where u is the twist factor. It follows from Eq. (5) that when $m=n=1$, the beam reduces to a TGSM beam [1, 2]. In other cases ($m>1$ or $n>1$), the beam carries high-order twist phase but it becomes spatially varying coherence states, i.e., the DOC depends on the special reference points one chooses. It should emphasize here that the coherence parameter δ_{0x}, δ_{0y} and twist factor u are intimately related through α, β and γ. Hence, they are not independent of each other. However, the CSD is always non-negative definiteness by choosing different sets of α, β and γ, and the value range of the twist factor for a given δ_0 satisfies $u^2\le 4/\delta_{0x}^{2m}\delta_{0y}^{2n}$. We term the beam having CSD function in Eq. (5) as the GHTPCBs. The DOC can be evaluated via the CSD function by the definition

$$\mu(\boldsymbol{r}_1,\boldsymbol{r}_2)=\frac{W(\boldsymbol{r}_1,\boldsymbol{r}_2)}{\sqrt{W(\boldsymbol{r}_1,\boldsymbol{r}_1)W(\boldsymbol{r}_2,\boldsymbol{r}_2)}}.\tag{6}$$

To investigate the influence of the beam orders m and n on the DOC in the source plane, we plot in Fig. 1 the theoretical results of the square of the DOC $|\mu(\boldsymbol{r}_1,0)|^2$ for the GHTPCBs with different beam orders m and n. The beam parameters used in the calculation are $\delta_{0x}=0.45^{1/m}$ mm, $\delta_{0y}=0.45^{1/n}$ mm and $u=8\ \mathrm{mm}^{-m-n}$ ($\alpha=1\ \mathrm{mm}^{-2}$, $\beta=1\ \mathrm{mm}^{-2}$ and $\gamma=4\ \mathrm{mm}^{-2}$). Note that the dimension of the twist factor u depends on the orders m and n, implying that the twist factor with different orders are physically different. Under the condition of the same order, the value of the twist factor reflects the strength of the twist phase. It is shown that different spatial correlation structures are constructed by taking different beam orders. When $m=n=1$, the DOC displays a circular Gaussian profile. Nevertheless, as the m or n increases, the DOC patterns turn into Cartesian symmetry. Especially for m and n larger than 2, the patterns become squares [see Figs. 1(d) and (e)].

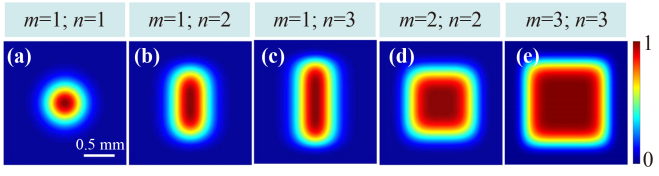

Fig. 1 Square of the DOC $|\mu(\boldsymbol{r}_1,0)|^2$ for GHTPCBs with different values of beam order m and n in the source plane.

3 Statistical properties of GHTPCBs on propagation

In this section, we will focus on the statistical properties of the GHTPCBs on propagation in free space. According to Eq. (2), the CSD function in the propagation plane z can be written as the following discrete modes:

$$W(\boldsymbol{\rho}_1,\boldsymbol{\rho}_2;z)\approx\sum_m^N\sum_n^N p(v_{xm},v_{yn})H_z^*(\boldsymbol{\rho}_1,v_{xm},v_{yn};z)\times H_z(\boldsymbol{\rho}_2,v_{xm},v_{yn};z)(\Delta v)^2,\tag{7}$$

where Δv is the discrete integral interval along the x and y directions. $N\times N$ represents the total number of discrete modes. It indicates from Eq. (7) the CSD function is expressed as the incoherent superposition of the light modes $\Phi_{mn}(\boldsymbol{\rho})=p^{1/2}(\boldsymbol{v}_{mn})H_z(\boldsymbol{\rho},\boldsymbol{v}_{mn};z)\Delta v$. Because the $p(\boldsymbol{v})$ decays with the increase of $|\boldsymbol{v}|$, finite number of the light modes could represent the theoretical model of the CSD function accurately. Based on the Huygens–Fresnel diffraction integral formula [32, 33], for each mode, the H_z function can be expressed as the following Fourier transform:

$$H_z(\boldsymbol{\rho},v_{xm},v_{yn};z)=-\frac{\mathrm{i}k}{2\pi z}\exp(\mathrm{i}kz)\exp\left(\frac{\mathrm{i}k}{2z}\boldsymbol{\rho}^2\right)\times F\left[H_0(\boldsymbol{r},v_{xm},v_{yn})\exp\left(\frac{\mathrm{i}k}{2z}\boldsymbol{r}^2\right)\right]_{\frac{\rho}{\lambda z}},\tag{8}$$

where F denotes the Fourier transform, allowing one to implement the Faster Fourier transform (FFT) algorithm to evaluate Eq. (8) using the MATLAB or others. The detailed derivation of Eq. (8) is shown in Supplementary Information S1.

Figure 2 illustrates the normalized spectral density $W(\boldsymbol{\rho},\boldsymbol{\rho};z)$ of the GHTPCBs for different beam orders m and n at several propagation distances in free space. The beam parameters used in the calculation are $u=8\ \mathrm{mm}^{-m-n}$, $\alpha=1\ \mathrm{mm}^{-2}$, $\beta=1\ \mathrm{mm}^{-2}$, $\gamma=4\ \mathrm{mm}^{-2}$ and $\sigma_0=0.5$ mm. In the calculation, the 30×30 modes are involved and the argument $\boldsymbol{v}$ is truncated in the range $[-2.5/\beta^{1/2},2.5/\beta^{1/2}]$. The $\boldsymbol{v}$ is discretized as $(v_{xm},v_{yn})=5/\beta^{1/2}(m/N,n/N)$, where m or n belongs to $[-N/2,N/2-1]$. For comparison, the spectral density of the TGSM beam (carrying conventional twist phase) upon propagation is also plotted [see Figs. 2(a1)–(a6) for $m=n=1$]. The spectral density remains Gaussian profile and keeps invariant during propagation, only the beam size expands due to the diffraction effect. As the order of the twist phase increases, there has a significant influence on the spectral density on propagation. The beam profile gradually turns into teardrop-like shape for $m=1$ and $n=2$, and diamond-like shape for $m=2$ and $n=2$. The beam is self-focused in y direction and stretched in x direction on propagation. In the case of

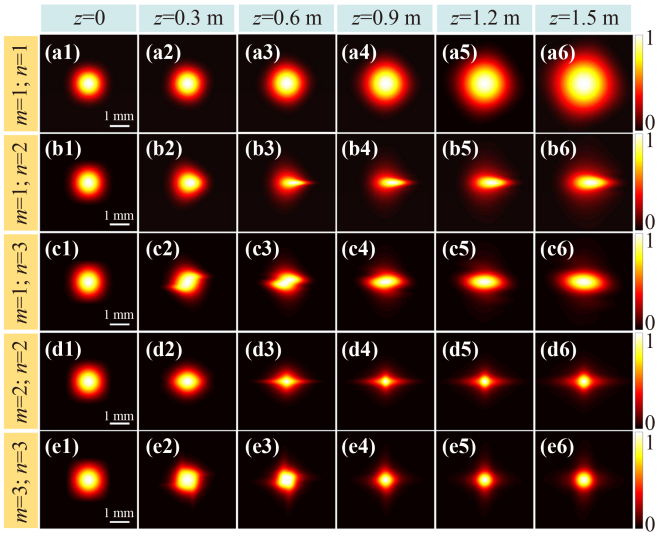

Fig. 2 Density plots of normalized spectral density of the GHTPCBs with $u = 8\ \mathrm{mm}^{-m-n}$ for different beam orders m and n at several propagation distances in free space.

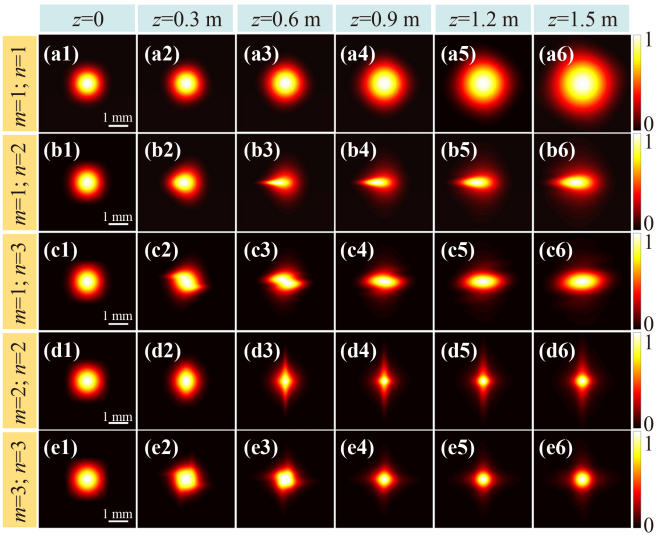

Fig. 3 Density plots of normalized spectral density of the GHTPCBs with $u = -8\ \mathrm{mm}^{-m-n}$ for different beam orders m and n at several propagation distances in free space.

$m = 1$ and $n = 3$, the beam profile evolves into elliptical shape with long and short axis along the x and y axis, respectively. In the case of $m = 3$ and $n = 3$, it is found that the spectral density at propagation distance $z = 1.5$ m returns to rotational symmetry, but the self-focusing occurs during propagation, i.e., the beam spot at $z = 1.5$ m is smaller than that in the source plane. In addition, we also plot the other spectral densities with different values of twist factor, and the results are shown in Supplementary Information S2. It was found that the value of twist factor also plays an important role in beam shaping. The influence of different twist factors on the beam during propagation has roughly the same trend, but with the increase of the twist factor, the beam shaping becomes more obvious. Therefore, the high-order twist phase provides a new degree of freedom to shape the beam profile through controlling the order and the magnitude of the phase.

In order to investigate the influence of the sign of the twist factor u on spectral density, Fig. 3 presents the spectral density of the GHTPCBs with different m and n at several propagation distances. The twist factor is chosen to be $u = -8\ \mathrm{mm}^{-m-n}$, and the other parameters are the same as those in Fig. 2. Compared Fig. 3 to Fig. 2, the effect of the sign of the twist factor on the spectral density depends on the orders of the twist phase. When $m = n = 2$, the spectral density just rotates 90 degree with respect to the propagation-axis between the positive and negative twist factor, whereas the spectral density flip horizontally in other cases. The different behaviors of the evolution of the spectral density between the positive and negative sign are closely related to the symmetry of the CSD. Suppose that the CSD of the GHTPCBs rotates angle θ counterclockwise with respect to coordinate origin. The relation between the new coordinate and old coordinate can be expressed by: $x_{i\theta} = x_i \cos\theta + y_i \sin\theta$ and $y_{i\theta} = -x_i \sin\theta + y_i \cos\theta$. On inserting the new coordinate into Eq. (5), it readily finds that when $m = n = 1$, the CSD is independent upon the angle θ. When $m = n = 2$, the CSDs between the positive and negative twist factor satisfies the condition $W^p(x_1, y_1, x_2, y_2) = W^n(y_1, -x_1, y_2, -x_2)$, where the superscript p and n denotes the case of the positive and negative twist factors, respectively. This symmetry of CSD results in the rotation of 90 degree of the spectral density between them. Other cases shown in Figs. 2 and 3, the CSDs between two signs of the twist factors are $W^p(x_1, y_1, x_2, y_2) = W^n(-x_1, y_1, -x_2, y_2)$ or $W^p(x_1, y_1, x_2, y_2) = W^n(x_1, -y_1, x_2, -y_2)$.

We now pay attention to the changes of the OAM flux density of the GHTPCBs upon free-space propagation. According to Ref. [28], the OAM flux density $M_d(\boldsymbol{\rho}; z)$ of a partially coherent beam at propagation distance z is expressed by the following formula:

$$M_d(\boldsymbol{\rho}; z) = \frac{\varepsilon_0}{k} \times \mathrm{Im}\left[\rho_{x1}\frac{\partial W(\boldsymbol{\rho}_1, \boldsymbol{\rho}_2; z)}{\partial \rho_{y2}} - \rho_{y1}\frac{\partial W(\boldsymbol{\rho}_1, \boldsymbol{\rho}_2; z)}{\partial \rho_{x2}}\right]_{\boldsymbol{\rho}_1 = \boldsymbol{\rho}_2}, \tag{9}$$

where ε_0 is the permittivity constant in vacuum. Im denotes taking the imaginary part. In the source plane $z = 0$, The z-component OAM flux density of the GHTPCBs has found the analytical formula by inserting Eq. (5) into Eq. (9):

$$M_d(\boldsymbol{r}; 0) = -\frac{A\varepsilon_0 u}{k}\exp\left(-\frac{\boldsymbol{r}^2}{2\sigma_0^2}\right) \times \left(nx^{m+1}y^{n-1} + my^{n+1}x^{m-1}\right), \tag{10}$$

where $A = 1/(2\sigma_0^2\pi)$ represents the normalized coefficient

of the CSD function. Therefore, the total average OAM flux per photon is calculated by the following formula:

$$t_d = \frac{\hbar\omega \int_{-\infty}^{\infty} M_d(\boldsymbol{r};0)\,\mathrm{d}^2\boldsymbol{r}}{A\sqrt{\varepsilon_0/\mu_0}\int_{-\infty}^{\infty} W(\boldsymbol{r},\boldsymbol{r};0)\,\mathrm{d}^2\boldsymbol{r}} = -\hbar u 2^{(m+n)/2-2}\sigma_0^{m+n} mn\Gamma\left(\frac{m}{2}\right)\Gamma\left(\frac{n}{2}\right) \times \left[1-(-1)^n-(-1)^m+(-1)^{m+n}\right]/\pi, \tag{11}$$

where $\hbar$ is the reduced Planck constant, μ_0 is the permeability in vacuum. ω is the angular frequency of the light beam. It indicates from Eq. (11) that if the beam order $m=n$ is even or $m+n$ is odd, the total OAM flux is zero. Owing to that the total OAM flux is conserved in free-space propagation, hence it remains zero unchanged at any propagation distance.

To evaluate the OAM flux density of the GHTPCBs propagation through free space, we insert Eqs. (7) and (8) into Eq. (9), and make some partial differential operations. The expression for the OAM flux density becomes

$$M_d(\boldsymbol{\rho};z) = \frac{A\varepsilon_0}{\lambda^2 z^2 k} \times \mathrm{Im}\sum_m^N\sum_n^N p(\boldsymbol{v}_{mn})\,F^{-1}\left[T^*(\boldsymbol{r}_1,\boldsymbol{v}_{mn})\right]_{\frac{\rho}{\lambda z}} \times \left\{\rho_x F\left[T(\boldsymbol{r}_2,\boldsymbol{v}_{mn})\left(-\frac{\mathrm{i}ky_2}{z}\right)\right]_{\frac{\rho}{\lambda z}} - \rho_y F\left[T(\boldsymbol{r}_2,\boldsymbol{v}_{mn})\left(-\frac{\mathrm{i}kx_2}{z}\right)\right]_{\frac{\rho}{\lambda z}}\right\}(\Delta v)^2, \tag{12}$$

with

$$T(\boldsymbol{r},\boldsymbol{v}_{mn}) = H_0(\boldsymbol{r},\boldsymbol{v}_{mn})\exp\left(\frac{\mathrm{i}k}{2z}\boldsymbol{r}^2\right), \tag{13}$$

where F^{-1} denotes the inverse Fourier transform. Based on Eqs. (12) and (13), the OAM flux density of the GHTPCBs on propagation can be numerically calculated with the help of FFT. In fact, Eq. (12) is applicable to calculate the OAM flux density of other kinds partially coherent beams if the $p(\boldsymbol{v})$ and $H_0(\boldsymbol{r},\boldsymbol{v})$ functions are known.

Figures 4 and 5 show the OAM flux density of the GHTPCBs with $u=8\,\mathrm{mm}^{-m-n}$ and $u=-8\,\mathrm{mm}^{-m-n}$ at several propagation distances, respectively. The other beam parameters used in the calculation are the same with those in Fig. 2. In the source plane, the OAM flux density between $u=8\,\mathrm{mm}^{-m-n}$ and $u=-8\,\mathrm{mm}^{-m-n}$ satisfies the relation $M_d(\boldsymbol{r},0)=-M_d(\boldsymbol{r},0)$, which also can be readily obtained from Eq. (10). The OAM flux density closely depends on the orders of the twist phase. Hence it provides one a way to control the OAM flux density through adjusting m and n. In the process of the free-space propagation, it can be seen that the OAM flux density shape keeps invariant only in the case of $m=n=1$. Other orders of the twist phase induce the changes of the OAM flux density on propagation. Some special patterns are formed during propagation. Compared Fig. 4 to Fig. 5, one finds that when $m=n=2$, the OAM flux density obeys the relation $M_d(x,y,z)=M_d(y,x,z)$ between positive and negative twist factors. Other cases for $m=1$, $n=2$; $m=1$, $n=3$ and $m=n=3$, the OAM flux density between positive and negative twist factors satisfies the relation $M_d(x,y,z)=-M_d(-x,y,z)$. An interesting phenomenon

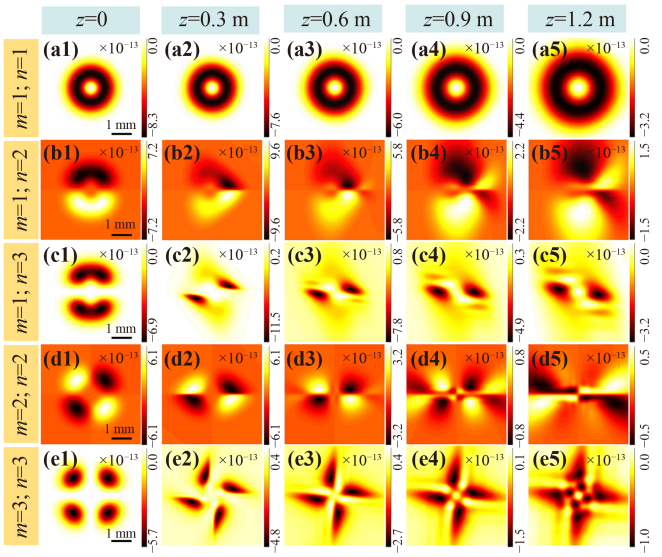

Fig. 4 Density plots of OAM flux density of the GHTPCBs with $u=8\,\mathrm{mm}^{-m-n}$ for different beam orders m and n at several propagation distances in free space.

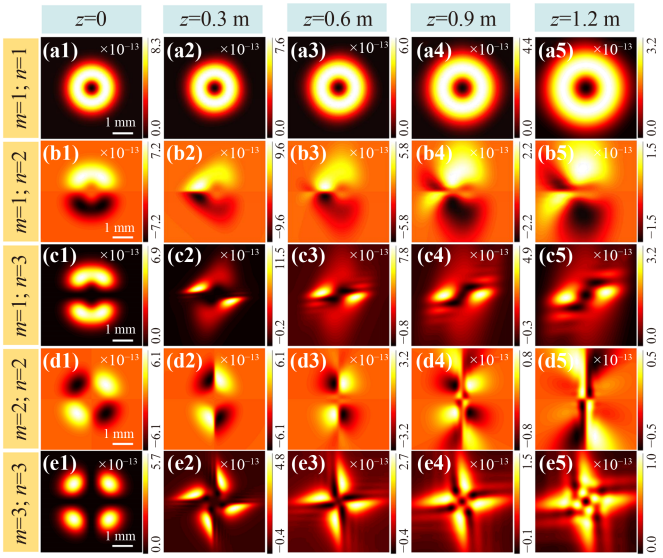

Fig. 5 Density plots of OAM flux density of the GHTPCBs with $u=-8\,\mathrm{mm}^{-m-n}$ for different beam orders m and n at several propagation distances in free space.

in the case of $m=n=3$ is that the OAM flux density evolves into a windmill-like shape on propagation, and the sign of the twist factor changes the orientation of each windmill leaf.

4 Experimental generation and propagation for GHTPCBs

In this section, we carry out the experimental generation of the GHTPCBs with controllable twist phase by means of the pseudo-mode superposition reported in Refs. [25, 34]. As we discussed in Section 3, the GHTPCBs can be represented as the superposition of spatially coherent, but mutually uncorrelated light modes [see Eq. (7)]. In the source plane, the light modes with indices m and n take the form $\Phi_{mn}(\boldsymbol{r}) = p^{1/2}(\boldsymbol{v}_{mn}) H_0(\boldsymbol{r}, \boldsymbol{v}_{mn}) \Delta v$. In order to realize the incoherent superposition of these modes in practical situation, a random phase $\exp(i\phi_{mn})$, where ϕ_{mn} is in the range of $0-2\pi$ with uniform probability distribution, is added into the mode $\Phi_{mn}(\boldsymbol{r})$. Therefore, the CSD function becomes

$$\begin{aligned} W(\boldsymbol{r}_1, \boldsymbol{r}_2) &= \sum_{m_1}^{N}\sum_{n_1}^{N}\sum_{m_2}^{N}\sum_{n_2}^{N} \Phi^*_{m_1 n_1}(\boldsymbol{r}_1)\Phi_{m_2 n_2}(\boldsymbol{r}_2) \\ &\times \langle \exp[-\mathrm{i}(\phi_{m_1 n_1} + \phi_{m_2 n_2})]\rangle \\ &= \sum_{m}^{N}\sum_{n}^{N} p(\boldsymbol{v}_{mn}) H_0^*(\boldsymbol{r}_1, \boldsymbol{v}_{mn}) H_0(\boldsymbol{r}_2, \boldsymbol{v}_{mn}) (\Delta v)^2 , \end{aligned} \tag{14}$$

In the derivation of Eq. (14), the relation $\langle \exp[-\mathrm{i}(\phi_{m1n1} + \phi_{m2n2})]\rangle = \delta_{m1m2}\delta_{n1n2}$ is applied, where δ is the Kronecker symbol. Compared Eq. (14) to Eq. (7), it was shown that the CSD function in this case has the same form as that in Eq. (7). In the experiment, one could encode the modes associated random phases, i.e.,

$$P_l(\mathbf{r}) = \sum_{m}^{N}\sum_{n}^{N} \sqrt{p(\boldsymbol{v}_{mn})} H_0(\boldsymbol{r}, \boldsymbol{v}_{mn}) \exp(\mathrm{i}\phi_{mn}) , \quad (l = 1, 2, 3, ..., L) , \tag{15}$$

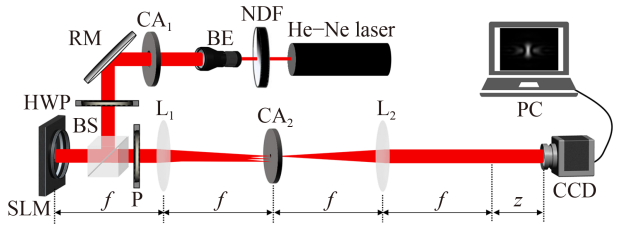

Fig. 6 Experimental setup for generating GHTPCBs via pseudo-mode superposition. NDF, neutral-density filter; BE, beam expander; CA_1, CA_2, circular apertures; RM, reflect mirror; HWP, half-wave plate; BS, beam splitter; SLM, spatial light modulator; P, linear polarizer; L_1, L_2, thin lenses; PC, personal computer; CCD, charge-coupled device.

into a spatial light modulator.

The experimental setup for the generation of the GHTPCBs is illustrated in Fig. 6. A linearly polarized laser beam ($\lambda = 632.8$ nm) generated by a He-Ne laser first passes through a neutral-density filter (NDF) and a beam expander (BE), then is reflected by a mirror (RM). The reflected beam passes through a half-wave plate (HWP), finally arrives at a phase-only spatial light modulator (SLM) with 1920×1080 pixels (HOLOEYE, PLUTO-VIS-130, pixel size: $8\ \mu\mathrm{m} \times 8\ \mu\mathrm{m}$) after reflected by a beam splitter (BS). The SLM acts as a modulator to modulate the amplitude and phase of the incident beam simultaneously. The method for the synthesis of computer-generated holograms (CGHs) loaded on the SLM is described in [26, 35]. Here, we adopt the method for synthesizing the CGH of type 3 described in Ref. [35]. The basic idea is as follows: we first write the phase-only CGH as the form $h(x,y) = \exp[\mathrm{i}\psi(A,\phi)]$, where ψ is the function of the prescribed amplitude A and phase ϕ. Note that A and ϕ are the spatially dependent. The $h(x,y)$ function is then expanded in terms of Fourier series and is associated with the phase modulation $\psi(A,\phi) = f(A)\sin(\phi)$ with $f(A)$ being an unknown function. Finally, the function $f(A)$ is solved by the equation $J_1[f(A)] = 0.582A$. Finally, the blazed grating is added onto the CGH to separate the desired beam and the other diffraction orders. The modulated light reflecting from the SLM passes through the BS again, entering a 4f optical system composed by lens L_1 and L_2 with both focal length being 15 cm. The polarizer (P) placed between the BS and L_1 is used to filter background noise in which the polarization direction does not coincide with that of the modulated beam. A circular aperture (CA_2) is located in the real focal plane of L_1 and is used to block other unwanted diffraction orders. Only the first order is allowed to pass through. The imaging plane of the 4f optical system is regarded as the source plane of the generated beam. In the experiment, the number of modes is chosen to be $L = 1000$. For each mode, there are 30×30 sub light modes which the selected manner is described in Section 3.

Figure 7 presents our experimental results of the modulus of the square of the DOC $|\mu(\boldsymbol{r}_1, 0)|^2$ of GHTPCBs with $u = 8\ \mathrm{mm}^{-m-n}$ for different beam orders m and n in the source plane. The beam parameters encoded into the CGHs are $\sigma_0 = 0.5$ mm, $\alpha = 1\ \mathrm{mm}^{-2}$ and

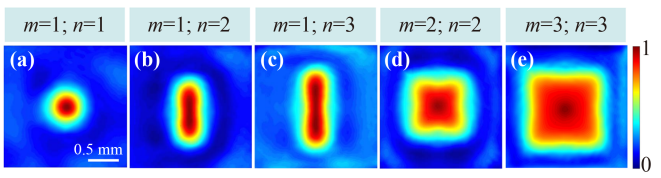

Fig. 7 Experimental results of square of the DOC $|\mu(\boldsymbol{r}_1, 0)|^2$ for GHTPCBs with different values of beam order m and n in the source plane.

$\beta = 1\ \mathrm{mm}^{-2}$. The results show that the DOC patterns indeed closely depend on the parameter m and n. As the m and n increases, the coherence area increases when a reference point is $\boldsymbol{r}_2 = 0$. The results are consistent with the theoretical predictions shown in Fig. 1.

Figure 8 presents the experimental results of the normalized spectral density for the generated beams $u = 8\ \mathrm{mm}^{-m-n}$ at different propagation distances. In the experiment, the CCD moves to the corresponding propagation distances z after the lens L_2, and records a series of instantaneous intensity distributions. The normalized spectral density is then averaged over the recorded intensity distribution for post data processing. Compared to the theoretical results shown in Fig. 2, one finds that the experimental results well agree with the theoretical results, except for slight speckle noise in the experiment. The other experimental results with $u = -8\ \mathrm{mm}^{-m-n}$ are shown in Supplementary Information S3, and they are all accordance with the theoretical predictions in Fig. 3.

5 Conclusion

In conclusion, we extend the high-order twist phase to a more general case, and the GHTPCBs are devised on the basis of the non-negative definiteness of the CSD function. The spectral density and the OAM flux density of the beams propagation in free space are studied through numerical examples. Our results shows that the orders of the twist phase have an important effect on the evolution of the spectral density and OAM flux density. The beam will focus self along x direction or y direction or both directions, depending on the indices m and n or the sign of the twist factor. Unlike the focusing of the beam by means of the Kerr effect in nonlinear medium, this self-focusing is a linear process without need of any medium. When the indexs m are not equal to n, the spectral densities during propagation are no longer Cartesian symmetry. Especially, a teardrop pattern is formed when $m = 1$ and $n = 2$. In addition, OAM flux density in free-space propagation is also closely related to the indices m and n. Through controlling the indices, some special patterns such as windmill-like structure and fluid rotator structure will be formed. The high-order twist phase and its orders provide a convenient way to tailoring the spectral density and OAM flux in light beams. Actually, due to the nonuniform intensity distribution of the GHTPCBs, that is, there exists intensity gradient, when the gradient force is much greater than the scattering force, particles can be stably captured at the position of maximum light intensity, and under the impetus of OAM, particles may be pushed into orbital motion. Furthermore, we report an experimental setup involving a phase-order SLM to generate the GHTPCBs with controllable twist phase. The spectral density during free-space propagation is measured in the experiment. It is shown that the experimental results agree well with the theoretical results. Our work may provide positive suggestions and useful applications for nonlinear optics due to the beam's self-focusing ability, and particle trapping based on its intensity and OAM property.

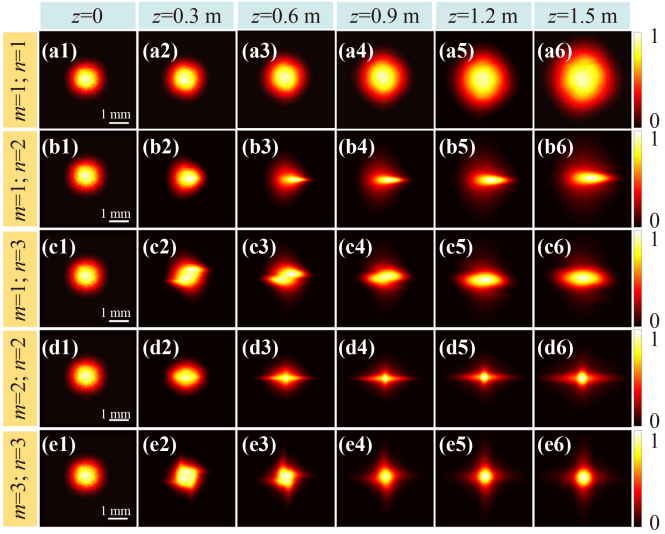

Fig. 8 Experimental results of the normalized spectral density of the GHTPCBs with $u = 8\ \mathrm{mm}^{-m-n}$ for different beam orders m and n at several propagation distances in free space.

Electronic supplementary materials are available in the online version of this article at https://doi.org/10.1007/s11467-022-1196-8 and https://journal.hep.com.cn/fop/EN/10.1007/s11467-022-1196-8 and are accessible for authorized users.

Acknowledgements This work was supported by the National Key Research and Development Program of China (Grant No. 2019YFA0705000); National Natural Science Foundation of China (Grant Nos. 11874046, 11974218, 11904247, 12104263, 12174279, and 12192254); Innovation Group of Jinan (No. 2018GXRC010); Local Science and Technology Development Project of the Central Government (No. YDZX20203700001766).

References

1. R. Simon and N. Mukunda, Twisted Gaussian Schell-model beams, *J. Opt. Soc. Am. A* 10(1), 95 (1993)
2. A. T. Friberg, E. Tervonen, and J. Turunen, Interpretation and experimental demonstration of twisted Gaussian Schell-model beams, *J. Opt. Soc. Am. A* 11(6), 1818 (1994)
3. K. Sundar, N. Mukunda, and R. Simon, Coherent-mode decomposition of general anisotropic Gaussian Schell-model beams, *J. Opt. Soc. Am. A* 12(3), 560 (1995)
4. D. Ambrosini, V. Bagini, F. Gori, and M. Santarsiero, Twisted Gaussian Schell-model beams: A superposition model, *J. Mod. Opt.* 41(7), 1391 (1994)

5. M. Bastiaans, Wigner distribution function applied to twisted Gaussian light propagating in first-order optical systems, *J. Opt. Soc. Am. A* 17(12), 2475 (2000)
6. Q. Lin and Y. Cai, Tensor ABCD law for partially coherent twisted anisotropic Gaussian–Schell model beams, *Opt. Lett.* 27(4), 216 (2002)
7. R. Borghi, F. Gori, G. Guattari, and M. Santarsiero, Twisted Schell-model beams with axial symmetry, *Opt. Lett.* 40(19), 4504 (2015)
8. R. Borghi, Twisting partially coherent light, *Opt. Lett.* 43(8), 1627 (2018)
9. F. Gori and M. Santarsiero, Devising genuine spatial correlation functions, *Opt. Lett.* 32(24), 3531 (2007)
10. F. Gori and M. Santarsiero, Devising genuine twisted cross-spectral densities, *Opt. Lett.* 43(3), 595 (2018)
11. Z. Mei and O. Korotkova, Random sources for rotating spectral densities, *Opt. Lett.* 42(2), 255 (2017)
12. G. Wu, Propagation properties of a radially polarized partially coherent twisted beam in free space, *J. Opt. Soc. Am. A Opt. Image Sci. Vis.* 33(3), 345 (2016)
13. Y. Zhou and D. Zhao, Propagation properties of a twisted rectangular multi-Gaussian Schell-model beam in free space and oceanic turbulence, *Appl. Opt.* 57(30), 8978 (2018)
14. C. Zhang, Z. Zhou, H. Xu, Z. Zhou, Y. Han, Y. Yuan, and J. Qu, Evolution properties of twisted Hermite Gaussian Schell-model beams in non-Kolmogorov turbulence, *Opt. Express* 30(3), 4071 (2022)
15. M. Santarsiero, F. Gori, and M. Alonzo, Higher-order twisted/astigmatic Gaussian Schell-model cross-spectral densities and their separability features, *Opt. Express* 27(6), 8554 (2019)
16. J. Zhang, J. Wang, H. Huang, H. Wang, S. Zhu, Z. Li, and J. Lu, Propagation characteristics of a twisted cosine-Gaussian correlated radially polarized beam, *Appl. Sci. (Basel)* 8(9), 1485 (2018)
17. B. Zhang, H. Huang, C. Xie, S. Zhu, and Z. Li, Twisted rectangular Laguerre–Gaussian correlated sources in anisotropic turbulent atmosphere, *Opt. Commun.* 459(15), 125004 (2019)
18. Y. Cai, Q. Lin, and O. Korotkova, Ghost imaging with twisted Gaussian Schell-model beam, *Opt. Express* 17(4), 2453 (2009)
19. S. A. Ponomarenko, Twisted Gaussian Schell-model solitons, *Phys. Rev. E* 64(3), 036618 (2001)
20. L. Wang, J. Wang, C. Yuan, G. Zheng, and Y. Chen, Beam wander of partially coherent twisted elliptical vortex beam in turbulence, *Optik (Stuttg.)* 218, 165037 (2020)
21. Z. Tong and O. Korotkova, Beyond the classical Rayleigh limit with twisted light, *Opt. Lett.* 37(13), 2595 (2012)
22. L. Hutter, G. Lima, and S. P. Walborn, Boosting entanglement generation in down-conversion with incoherent illumination, *Phys. Rev. Lett.* 125(19), 193602 (2020)
23. G. H. dos Santos, A. G. de Oliveira, N. Rubiano da Silva, G. Cañas, E. S. Gómez, S. Joshi, Y. Ismail, P. H. Souto Ribeiro, and S. P. Walborn, Phase conjugation of twisted Gaussian Schell model beams in stimulated down-conversion, *Nanophotonics* 11(4), 763 (2022)
24. H. Wang, X. Peng, L. Liu, F. Wang, Y. Cai, and S. A. Ponomarenko, Generating bona fide twisted Gaussian Schell-model beams, *Opt. Lett.* 44(15), 3709 (2019)
25. C. Tian, S. Zhu, H. Huang, Y. Cai, and Z. Li, Customizing twisted Schell-model beams, *Opt. Lett.* 45(20), 5880 (2020)
26. H. Wang, X. Peng, H. Zhang, L. Liu, Y. Chen, F. Wang, and Y. Cai, Experimental synthesis of partially coherent beam with controllable twist phase and measuring its orbital angular momentum, *Nanophotonics* 11(4), 689 (2022)
27. J. Serna and J. M. Movilla, Orbital angular momentum of partially coherent beams, *Opt. Lett.* 26(7), 405 (2001)
28. S. M. Kim and G. Gbur, Angular momentum conservation in partially coherent wave fields, *Phys. Rev. A* 86(4), 043814 (2012)
29. Y. Cai and S. Zhu, Orbital angular moment of a partially coherent beam propagating through an astigmatic ABCD optical system with loss or gain, *Opt. Lett.* 39(7), 1968 (2014)
30. L. Liu, Y. Huang, Y. Chen, L. Guo, and Y. Cai, Orbital angular moment of an electromagnetic Gaussian Schell model beam with a twist phase, *Opt. Express* 23(23), 30283 (2015)
31. L. Wan and D. Zhao, Generalized partially coherent beams with nonseparable phases, *Opt. Lett.* 44(19), 4714 (2019)
32. S. A. Collins, Lens-system diffraction integral written in terms of matrix optics, *J. Opt. Soc. Am.* 60(9), 1168 (1970)
33. L. Mandel and E. Wolf, Optical Coherence and Quantum Optics, Cambridge University Press, 1995
34. R. Wang, S. Zhu, Y. Chen, H. Huang, Z. Li, and Y. Cai, Experimental synthesis of partially coherent sources, *Opt. Lett.* 45(7), 1874 (2020)
35. V. Arrizón, U. Ruiz, R. Carrada, and L. A. González, Pixelated phase computer holograms for the accurate encoding of scalar complex fields, *J. Opt. Soc. Am. A* 24(11), 3500 (2007)